Aerodynamic design of a high aspect ratio strut-braced wing

Diego Losada Costoso, Eric Nguyen Van, Olivier Atinault, Michaël Méheut

▶ **To cite this version:**

Diego Losada Costoso, Eric Nguyen Van, Olivier Atinault, Michaël Méheut. Aerodynamic design of a high aspect ratio strut-braced wing. ECCOMAS 2024, Jun 2024, Lisbonne, Portugal. 10.23967/eccomas.2024.145 . hal-04759883

HAL Id: hal-04759883
https://hal.science/hal-04759883v1

Submitted on 30 Oct 2024

HAL is a multi-disciplinary open access archive for the deposit and dissemination of scientific research documents, whether they are published or not. The documents may come from teaching and research institutions in France or abroad, or from public or private research centers.

L'archive ouverte pluridisciplinaire **HAL**, est destinée au dépôt et à la diffusion de documents scientifiques de niveau recherche, publiés ou non, émanant des établissements d'enseignement et de recherche français ou étrangers, des laboratoires publics ou privés.

Distributed under a Creative Commons Attribution - NonCommercial - ShareAlike 4.0 International License

The 9th European Congress on Computational Methods in Applied Sciences and Engineering
ECCOMAS Congress 2024
3 – 7 June 2024, Lisboa, Portugal

AERODYNAMIC DESIGN OF A HIGH ASPECT RATIO STRUT-BRACED WING

D. LOSADA COSTOSO[1], E. NGUYEN VAN[2], O. ATINAULT[3] AND M. MÉHEUT[4]

1 ONERA, DAAA, ONERA, Institut Polytechnique de Paris, 92190, Meudon, France,
diego.losada_costoso@onera.fr
2 ONERA, Université de Toulouse, 2 Av. Edouard Belin, 31000 Toulouse, France,
eric.nguyen_van@onera.fr
3 ONERA, DAAA, ONERA, Institut Polytechnique de Paris, 92190, Meudon, France,
olivier.atinault@onera.fr
4 ONERA, DAAA, ONERA, Institut Polytechnique de Paris, 92190, Meudon, France,
michael.meheut@onera.fr

Key Words: *strut-braced wing, aerodynamic design, airfoil, optimization, CFD*

Summary. As part of Clean Aviation's UPWING project, the present work aims at designing a hydrogen-powered transport aircraft for a Short-Medium Range mission (239 PAX, 2500 NM) while reducing its overall energy consumption compared to existing aircraft. From an aerodynamic point of view, one way to reduce drag is to use higher aspect ratio wing [1]. The present work focuses on the transonic aerodynamic design of a strut-braced high-aspect-ratio wing configuration. The study begins with the overall aircraft study, which provides a preliminary design with the general shape of the aircraft (positions and dimensions of the horizontal and vertical stabilizers, wing and fuselage), based on conceptual design assumptions. Then, the design process uses the ESP/CAPS CAD modeler [2] and creates a geometry, which is used to design and assess the aerodynamic performance of the configuration (with automatic meshing, CFD RANS simulation and Far-Field Drag analysis [4]). The aerodynamic wing design also includes an airfoil optimization step. The preliminary design takes into account structural constraints into consideration defined from low fidelity models. The aerodynamic performance of the optimized shape will be analyzed in cruise and off-design conditions.

1 INTRODUCTION

As part of Clean Aviation's UPWING project, the present work aims at designing a hydrogen-powered transport strut-braced wing aircraft for a Short-Medium Range mission (239 PAX, 2500 NM), while reducing its overall energy consumption compared to existing aircraft. For this study, the Mach number is fixed at 0.78 and the lift coefficient at 0.650 (M=0.78, C_L=0.650). This lift coefficient was defined by the Overall Aircraft process from the aircraft weight in cruise and the wing surface. To reduce the aircraft energy consumption, it is necessary to reduce its drag. One way of achieving this, is to design a high aspect ratio wing configuration to reduce the induced drag generated by the aircraft. The induced drag represents about one third of the total drag of a conventional transonic aircraft. However, increasing the aspect ratio generates very long wings, and consequently the bending moment at the root and the wing weight become very high, as shown in Figure 1 [1]. The advantage of the strut-braced wing is

therefore to increase the aspect ratio of the wing while maintaining an acceptable bending moment at the root.

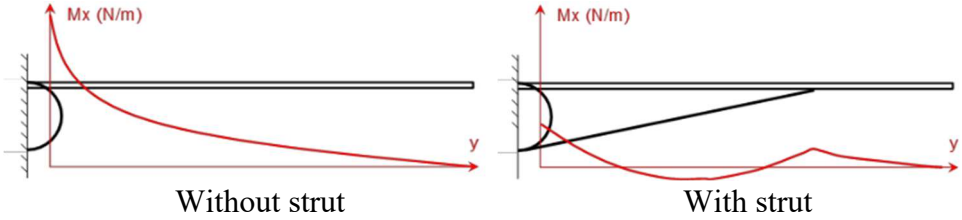

Figure 1: Effect of adding a strut on the wing root bending moment.

However, designing a strut-braced wing involves complex and innovative structural and aerodynamic design challenges.

In this process, the aircraft is sized according to Top Level Requirements such as the number of passengers, cruise Mach number and range. It relies on a collection of multi-disciplinary analytical and semi-empirical models and a time simulation for the mission. The FAST-OAD version used for this study makes use of additional modules to take into account a strut-braced wing (model in [3]) and a hydrogen propulsion system with the tank located in the rear part of the fuselage. The detailed aerodynamic design however is not made in FAST-OAD and is the subject of the present study. The wing planform given by the Overall Aircraft Design process is shown on Figure 2 and Table 1. The aerodynamic design is divided into two main steps. First, the focus is on the wing: the design of the 3D wing is performed using a step-by-step approach: airfoil optimization, 3D wing definition based on optimized airfoil and OAD planform then

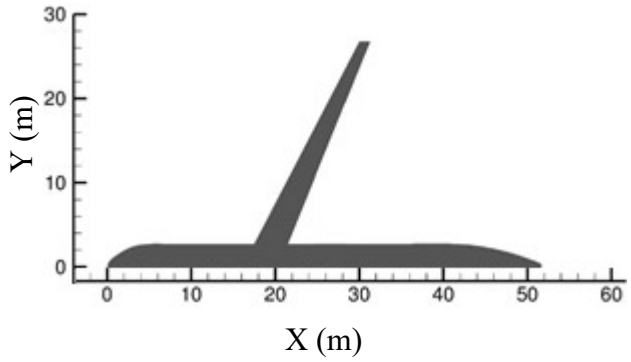

Figure 2: Planform given by OAD.

Table 1: Geometric data from OAD study.

Wing: Aspect ratio	19.0
Wing: Span	53.6m
Wing: Leading edge sweep angle	27.5°
Wing: Ref. area	151.2m
Wing: Taper ratio	0.3m
Fuselage: Diameter	5.5m
Fuselage: Length	51.7m

spanwise twist optimization. The second step focuses on the strut design with the definition of twist law and the strut load distribution, as well as the strut-wing junction.

In the following sections, the tools and methods used in the study are first described, then the aerodynamic shape design is exposed, and some perspectives are given.

2 TOOLS AND PROCESS

We will first define the optimization problem that will be used in Section 3, and we will then describe the 3D aerodynamic design framework used in this study.

2.1 2D Airfoil optimization

A multipoint optimization on two flight points was performed: cruise flight (pt1: M=0.78, C_L=0.650) and flight at MMO (Mach Maximum Operating) (pt2: M=0.82, C_L=0.580). Here, a gradient-based optimization is used, using finite differences to calculate sensitivities. The objective function is defined as a linear combination of the drag at the two flight points weighted by a coefficient K such as:

$$F_{obj} = C_{d_{pt1}} * K + (1 - K) * C_{d_{pt2}} \quad (1)$$

Regarding the constraints imposed during the optimization, we have a lift constraint on each flight points, a constraint on the airfoil pitching moment and a geometric constraint on minimum thickness.

The optimization variables are composed of 5 geometric variables as well as the angle of incidence for each flight point. The geometric variables used are the airfoil leading-edge radius, the maximum upper side and lower side thicknesses, and the upper side and lower side outlet angles. These geometric variables are shown in Figure 3 and examples of airfoil deformation are presented in Figure 4. To evaluate airfoil performance, a CFD Euler solver coupled with a boundary layer approach is used [4]. The complete multipoint optimization loop is summarized in Figure 5. This optimization loop is a classic multipoint optimization loop.

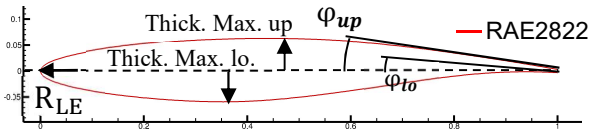

Figure 3: Geometric variables used for the optimization.

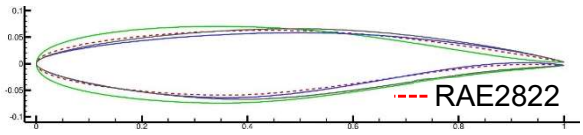

Figure 4: Examples of airfoil deformations.

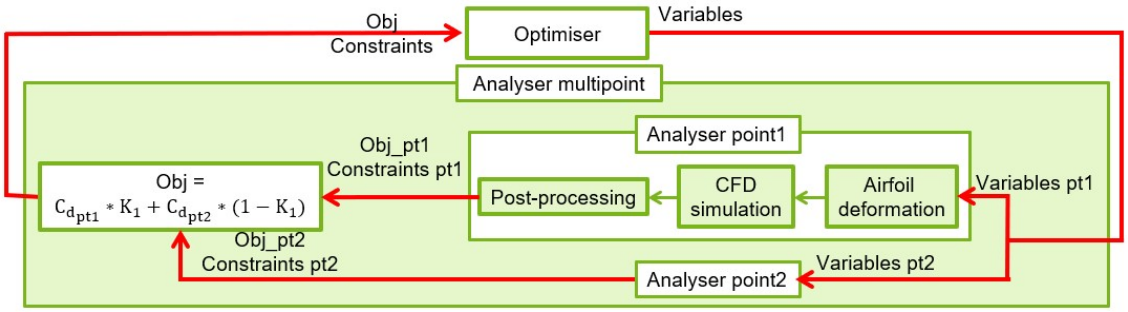

Figure 5: Multipoint optimization loop.

2.2 3D Aerodynamic design framework

For the three-dimensional aerodynamic design of the aircraft, the design framework presented in Figure 6 [1] is used. First, the Engineering Sketch Pad (ESP) [2] tool developed by MIT generates a parametric 3D CAD model. This geometry is then automatically meshed using Pointwise software. After the meshing step, the CFD computation, Euler or RANS, is performed using the SU_2 solver [5]. Finally, in order to post-process the CFD computation, the ONERA Far-Field Drag post-processor FFD [6] is used to evaluate the different contributions of drag (induced drag, wave drag, viscous pressure drag, friction drag) with accuracy.

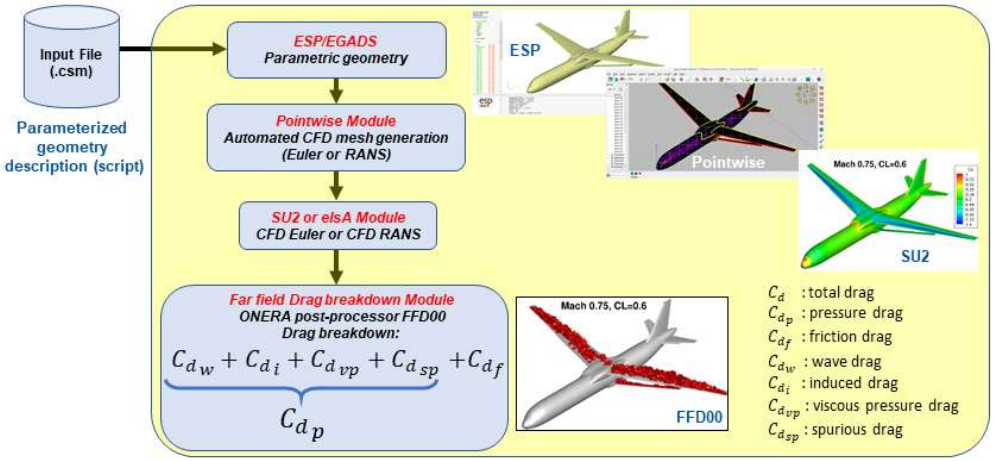

Figure 6: 3D aerodynamic framework used.

On the next sections of this paper, we will use the isentropic Mach number to visualize the surface fields of the flow. The isentropic Mach number is defined by:

$$M\_is = \sqrt{\frac{2}{\gamma - 1}\left(\left(\frac{P_{0\infty}}{P}\right)^{\frac{\gamma-1}{\gamma}} - 1\right)} \quad (2)$$

- γ is the ratio of specific heats ($\gamma = 1.4$)
- $P_{0\infty}$ is the total pressure in the freestream
- P is the local Static pressure

3 DESIGN OF THE STRUT-BRACED WING CONFIGURATION

To begin with, we will describe the work that went into designing the wing in two steps. The first one is about the optimization of wing airfoils, while the second one involves the development of a wing twist law and the study of the spanwise load distribution. After designing the wing, we will move on to the design of the strut and the strut-wing junction.

3.1 Wing design

Throughout this section, the wing is designed first without considering the strut.

3.1.1 Airfoil optimization

The multipoint optimization process is initialized with an airfoil that results from a single point optimization performed with the airfoil of the U-HARWARD [7] concept. As a reminder, two flight points are considered: cruise flight (pt1: M=0.78, C_L=0.650) and flight at MMO (pt2: M=0.82, C_L=0.580). The non-optimized and optimized airfoils are shown in Figure 7. Figure 8 shows the pressure distributions on these two airfoils for the two flight points. As can be seen

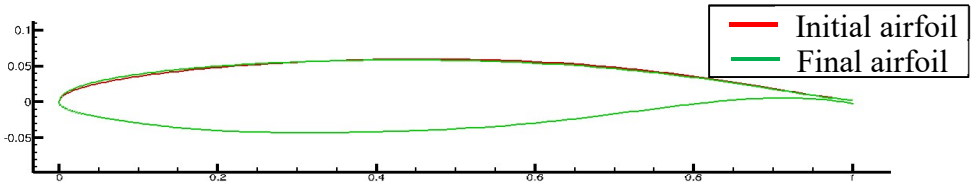

Figure 7: Optimized and non-optimized airfoils geometry.

from the Table 2, there is a deterioration of the performance in cruise but a significant improvement at MMO. This is mostly due to the wave drag, which follows the same trend. This effect is clearly visible on the pressure distribution shown in Figure 8. At MMO (pt2) we obtain an 8.5 drag counts (d.c.) reduction on wave drag with the optimized airfoil, while the shock is increased at cruise conditions (pt1), adding 11.3 d.c to the wave drag.

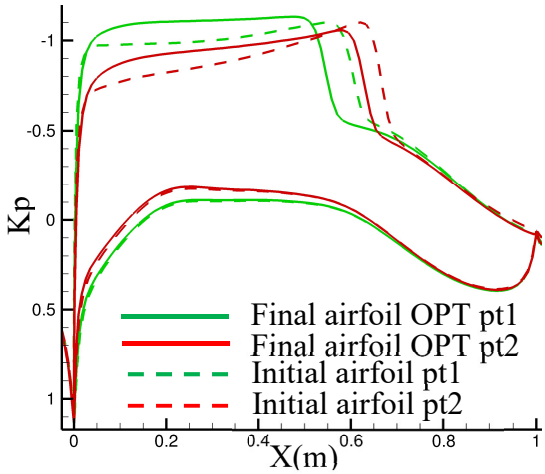

Figure 8: Pressure coefficient distribution at cruise and MMO conditions for the optimized and non-optimized airfoils.

Table 2: Multipoint optimization results.

Initial airfoil (before multipoint opt.)

	Cruise Pt1	MMO Pt2
C_D	125.5e-04	155.5e-04
C_{D_w}	16.7e-04	35.2e-04
C_l	0.810	0.710

Final airfoil (after multipoint opt.)

	Cruise Pt1	MMO Pt2
C_D	134.0e-02	135.1e-02
C_{D_w}	28.0e-04	26.7e-04
C_l	0.810	0.711

To compare the behavior of these two airfoils on a three-dimensional wing, it is possible to build one using the planform provided by the OAD and a twist law giving an elliptical load distribution along the spanwise. Table 3 and Table 4 show the performances of both wings generated by the airfoils for cruise conditions and MMO conditions. On these 3D wings, the same behavior is observed as on the airfoils. At cruise conditions, a slight deterioration of the wing performance is obtained with the optimized airfoil. At MMO, however, the wing performance is enhanced by the optimized airfoil. The impact on performance is mainly due to the wave drag and viscous pressure drag components. At MMO, the shock attenuation on the wing leads to a reduction in the thickening of the boundary layer across the shock wave. In this

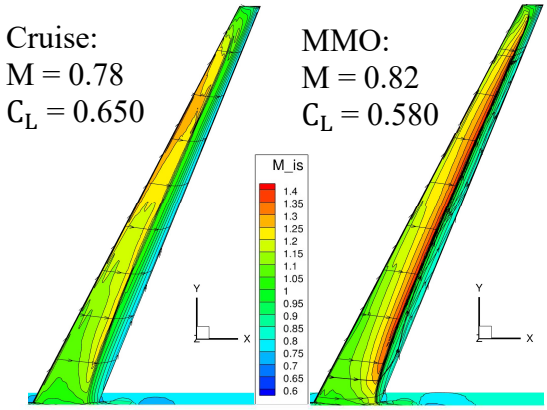

Figure 9: Non-optimized airfoils on three-dimensional wing.

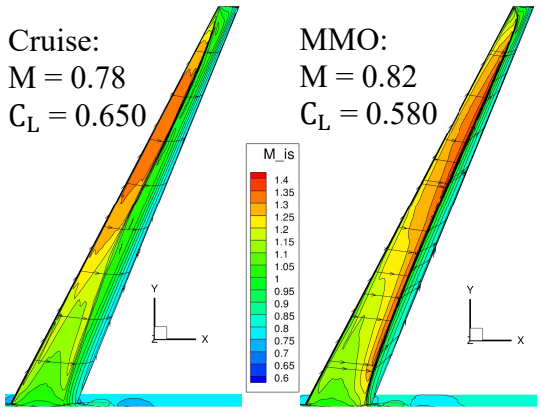

Figure 10: Optimized airfoils on three-dimensional wing.

Table 3: Performances of the three-dimensional wing with the optimized airfoil and non-optimized airfoil at cruise conditions.

C_D in d.c.

Twist law	Non-optim. airfoil	Multipoint optim. airfoil
AoA (°)	1.64	1.67
C_D	269.4	278.0
C_{D_w}	1.07	4.91
$C_{D_{vp}}$	47.7	49.1
C_{D_i}	74.3	74.3
C_{D_f}	149.7	149.7
Oswald	0.953	0.953
L/D	24.1	23.4

Table 4: Performances of the three-dimensional wing with the optimized airfoil and non-optimized airfoil at MMO conditions.

C_D in d.c.

Twist law	Non-optim. airfoil	Multipoint optim. airfoil
AoA (°)	1.04	0.95
C_D	319.5	301.07
C_{D_w}	40.3	31.4
$C_{D_{vp}}$	70.72	61.06
C_{D_i}	62.14	62.31
C_{D_f}	146.3	146.3
Oswald	0.931	0.929
L/D	18.61	19.53

way, the reduction in wave drag induces the reduction on the viscous pressure drag. Still at MMO, the skin friction lines are strongly deviated on the wing equipped with the non-optimized airfoil. This indicates flow separation downstream of the shock wave on the wing. With the optimized airfoil, this deviation is greatly attenuated, resulting in a better wing behavior for these flight conditions. At cruise, the slight deterioration in performance can be seen on the isentropic Mach number field. In fact, the high-speed zone about two-thirds of the wing span is larger and more intense with the optimized airfoil. In the rest of the study, the optimized multipoint airfoil will be used to generate the wing.

3.1.2 Spanwise load distribution and twist law

This section focuses on the definition of the wing twist law. For this, the optimized multipoint airfoil developed in section 3.1.1 is used. Figure 11 shows the twist laws tested. The best twist law shown in Figure 11 has been developed in order to reduce the aircraft drag as much as possible, by finding a good compromise between reducing wave drag and reducing induced drag. The load distribution of the DLR F25 is given as an example.

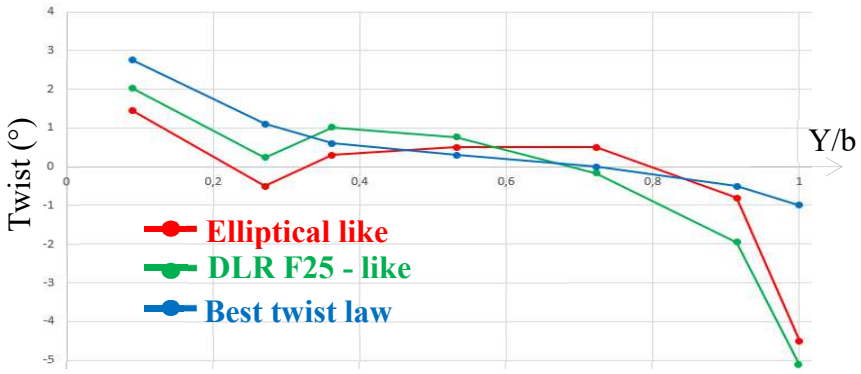

Figure 11: Spanwise twist distributions.

Table 5: Impact of the spanwise twist distributions on the aerodynamic performance in cruise.

C_D in d.c.

Twist law	AoA (°)	C_D	C_{D_w}	C_{D_i}	$C_{D_{vp}}$	C_{D_f}	Oswald	L/D
Like Ellip. load	1.67	278.0	4.9	74.3	49.1	149.7	0.953	23.4
Like DLR F25 load	1.42	278.0	3.4	76.0	48.5	151.9	0.931	23.2
Best twist law	1.14	275.6	0.9	76.9	47.4	150.4	0.920	23.6

Table 6: Impact of the spanwise twist distributions on the aerodynamic performance at MMO.

C_D in d.c.

Twist law	AoA (°)	C_D	C_{D_w}	C_{D_i}	$C_{D_{vp}}$	C_{D_f}	Oswald	L/D
Ellip. like load	0.96	301.1	31.4	62.3	61.1	146.3	0.904	19.26
DLR F25 - like load	0.65	299.9	28.8	62.7	59.6	148.6	0.898	19.34
Best twist law	0.34	289.6	22.8	63.6	55.8	147.3	0.886	20.03

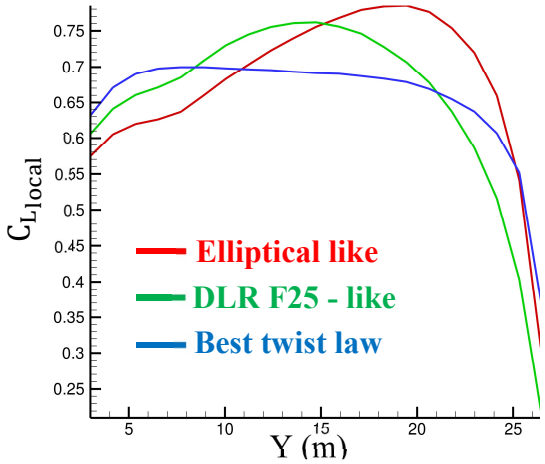

Figure 12: Spanwise local lift coefficient distributions in cruise conditions.

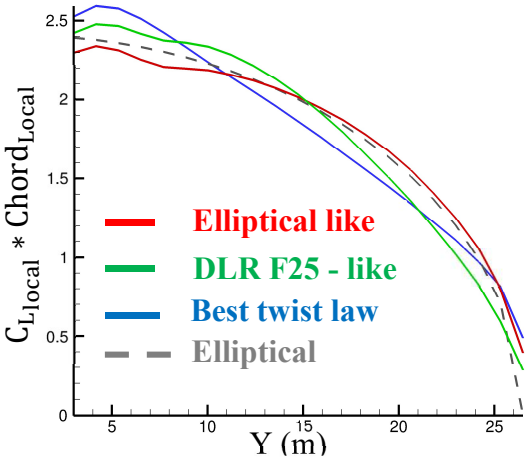

Figure 13: Spanwise load distributions in cruise conditions.

The "Elliptical like" load distribution was developed as a first step in the design process. This "Elliptical like", is the one used in section 3.1.1 to generate the wing. Figure 12 and Figure 13 show respectively the local lift coefficients and span load distribution generated by these twist laws. Table 5 and Table 6 show the performances of these 3 twist laws at cruise and MMO conditions. Figure 14 show the isentropic Mach number field on which the skin friction lines are superimposed for both flight conditions considered. The elliptical and DLR F25-like load distributions create a zone of very high local lift, generating high-speed zones and shocks on the upper surface of the wing, as shown in Figure 12. These very high local lift coefficients therefore generate the wave drag shown in Table 5 and Table 6. With the best twist law, this local lift coefficients curve is flattened, the inner wing is more loaded and the local lift peak, as well as the high-speed zones on the upper surface of the wing, are eliminated. This best twist law not only reduces wave drag, but also the thickening of boundary layers downstream of the

shock, and therefore viscous pressure drag. Regarding the spanwise load distribution, Figure 13 shows that the best twist law is moving away from the elliptical load distribution. In Table

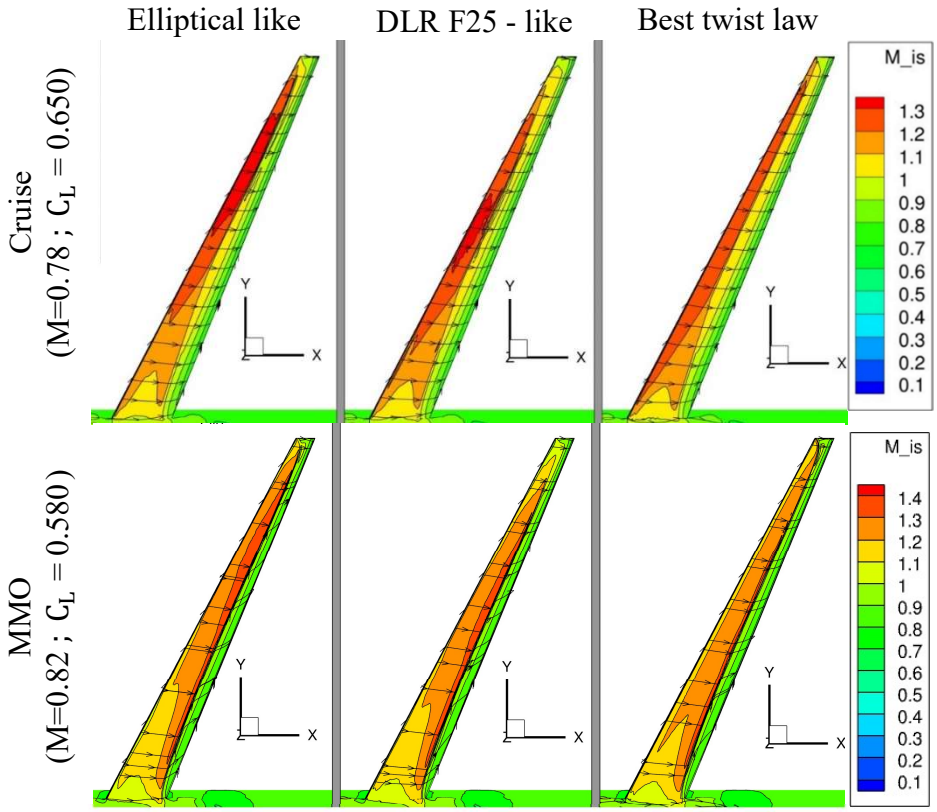

Figure 14: Isentropic Mach number field at cruise (up) and MMO (down) conditions.

5 and Table 6, this results in a slight deterioration in the induced drag for the wing using the best twist law. With the combination of these effects, the use of the best twist law is beneficial. Indeed, the best twist law improves the lift over drag ratio. In the final design, this best twist law will be used.

3.2 Strut design

In this section, we will focus on the strut design. First, the strut twist law will be defined, then the design of the strut-wing junction will be studied. The strut is generated using the symmetrical airfoil NASA SC20010 shown in Figure 15. The thickness of this airfoil is 10%.

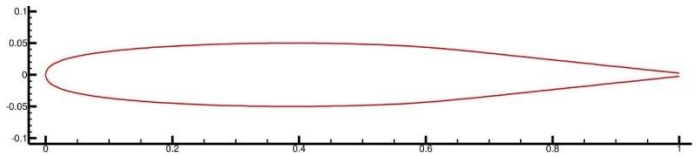

Figure 15: Strut airfoil (NASA SC20010).

3.2.1 Strut twist law and load distribution

In this section, the strut twist law is defined to obtain a non-lifting strut. Figure 16 shows the

original and the best strut twist laws. As shown in Figure 16, the original strut design produces slightly negative lift over most of its span, with a local lift peak close to the strut-wing junction. A negative lifting strut is absolutely not advantageous, as in this case the wing has to compensate by producing more lift, and consequently lift-induced drag, wave drag and viscous pressure drag increase. With the best strut twist law shown in Figure 17, the desired non-lifting

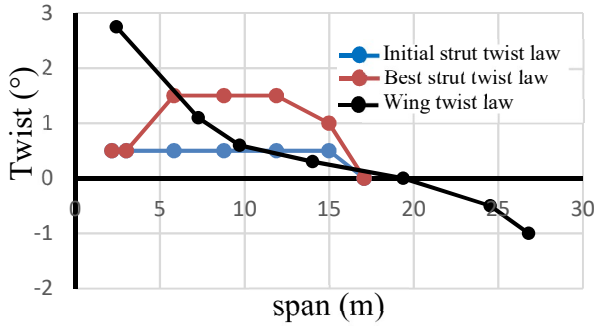

Figure 16: Wing and strut twist laws.

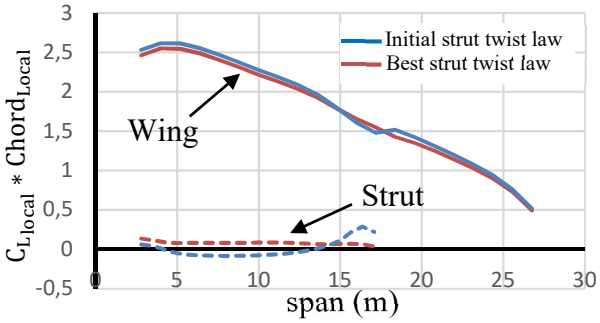

Figure 17: Load distribution on the strut and the wing in cruise conditions.

Table 7: Performances of the original and the best strut twist law.

C_D in d.c.

Twist law	AoA (°)	C_D	C_{D_w}	C_{D_i}	$C_{D_{vp}}$	C_{D_f}	Oswald	L/D
Initial strut twist law	1.10	299.3	0.1	78.9	57.9	162.4	0.898	21.7
Best strut twist law	0.94	296.6	0.0	78.6	56.5	162.5	0.901	21.9

strut is obtained. As shown in Table 7, this new design mainly reduces viscous pressure drag, and more slightly the induced drag and the wave drag. This result is contradictory with the work presented by Secco, N. R., & Martins, J. R [8]. However, the geometric differences on the strut and the wing (sweep angle, dihedral, etc.) could explain the differences in the behavior observed here. An in-depth analysis would therefore be necessary to gain a good understanding of this behavior.

3.2.2 Strut-wing junction design

In this section, we focus on the aerodynamic behavior of the strut-wing junction. Figure 19 and Figure 18 show the original design and the new design of the strut-wing junction in cruise conditions. As shown in Figure 19 due to the interaction between the wing and strut boundary layers and the interaction of these boundary layers with the shock wave, a separation

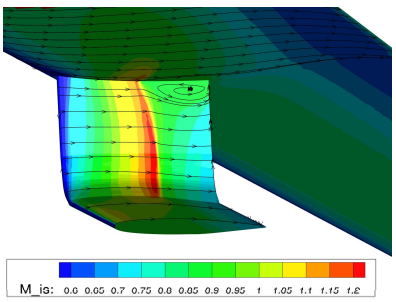

Figure 19: Original strut-wing junction design.

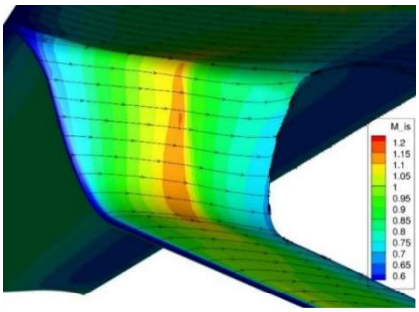

Figure 18: New strut-wing junction design.

downstream of the shock is observed. Due to these phenomena, the design of this zone is highly complex. Several modifications have been applied to improve the aerodynamic behavior of the strut-wing junction. As shown in Figure 18, sweep has been added to the vertical part of the strut and the chord was extended conserving the same absolute thickness of the airfoils. Finally, a fairing has been designed at the strut-wing junction. Thanks to this new design, at cruise conditions, the interaction between the shock and the boundary layers is greatly attenuated, and the resulting flow separation has been removed.

3.3 Performance of the final configuration

In this section, we will focus on the performances at cruise and at MMO conditions of the aerodynamic shape described in the previous sections.

3.3.1 Performance at cruise conditions

Figure 20 shows the isentropic Mach number field and the skin friction lines on the upper surface of the wing at cruise conditions (M=0.78, C_L=0.650). Figure 21 and Figure 22 show respectively the inner and outer parts of the strut-wing junction. Table 8 shows the performance of this aerodynamic shape at cruise conditions. As can be seen at cruise speed, the flow on the wing is clean, there is no shock or separation. With regard to the strut-wing junction, as explained in section 3.2.2, this design reduces shock-boundary layer interaction and eliminates the flow separation at the junction. Regarding the performance shown in Table 8, this configuration does not generate wave drag at cruise flight. It is also possible to see that the lift-drag ratio is not large enough for an aircraft with a high aspect ratio wing of 19. Here, the drag,

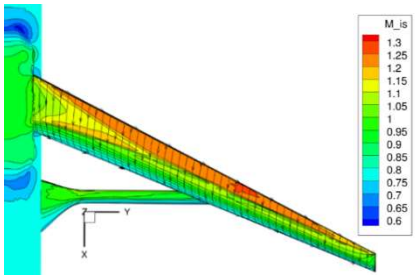

Figure 20: Isentropic Mach number field on the wing of the final configuration at cruise conditions.

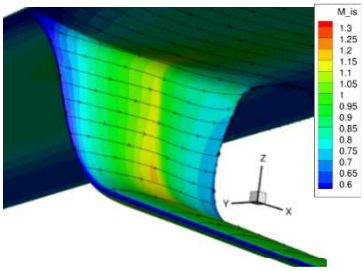

Figure 21: Isentropic Mach number field on the inner part of the strut-wing junction of the final configuration at cruise conditions.

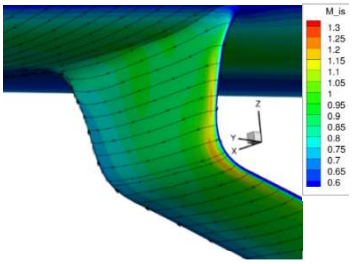

Figure 22: Isentropic Mach number field on the outer part of the strut-wing junction of the final configuration at cruise conditions.

Table 8: Performance of the final configuration at cruise conditions.

C_D in d.c.

	AoA (°)	C_D	C_{D_w}	C_{D_i}	$C_{D_{vp}}$	C_{D_f}	Oswald	L/D	L/D Classic fus.
Final conf.	0.941	296.61	0.0	78.1	55.2	193.3	0.907	21.9	23.0

and hence lift-drag ratio, is penalized by the fuselage drag. Indeed, the fuselage diameter is 5.5 meters and 55 meters long to accommodate the hydrogen tanks. For a conventional aircraft fuselage carrying out the same mission (such as the Airbus A320), the diameter would be 4.5 meters and the length would be 44.5 meters. Thus, this 19-aspect ratio strut-braced wing with

a conventional fuselage would have an estimated lift-drag ratio of around 23 at cruise.

3.3.2 Performance at MMO conditions

Figure 24 shows the isentropic Mach number field and the skin friction lines on the upper surface of the wing at the MMO conditions (M=0.82, C_L=0.580). Figure 23 and Figure 25 show respectively the inner and outer parts of the strut-wing junction. Table 9 shows the performance of this aerodynamic shape at the MMO conditions. As shown in Figure 24, on the wing at the

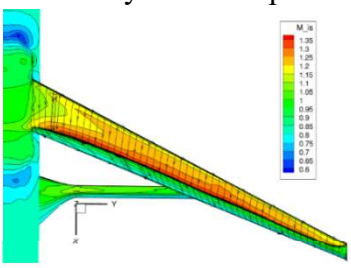

Figure 24: Isentropic Mach number field on the wing of the final configuration at MMO conditions.

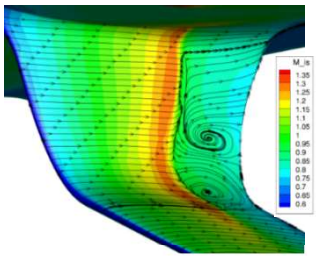

Figure 23: Isentropic Mach number field on the inner part of the strut-wing junction of the final configuration at MMO conditions.

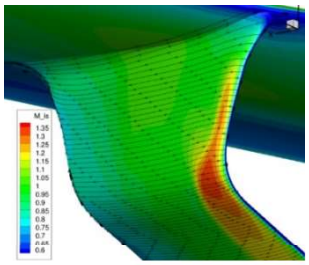

Figure 25: Isentropic Mach number field on the outer part of the strut-wing junction of the final configuration at MMO conditions.

Table 9: Performance of the final configuration at MMO conditions.

C_D in d.c.

	AoA (°)	C_D	C_{D_w}	C_{D_i}	$C_{D_{vp}}$	C_{D_f}	Oswald	L/D	L/D Classic fus.
Final conf.	0.29	319.2	25.6	64.1	70.0	159.5	0.879	18.2	18.5

MMO, a shock is present on a large part of the wing span. On the inner wing, as can be seen in Figure 24, the skin friction lines are deflected, indicating that the flow is close to separation or even already slightly separated. Regarding the aerodynamic behavior of the strut-wing junction under these conditions, the shock-boundary layer interaction leads to a strong flow separation downstream of the shock. In the same way as for cruise conditions, performance, and therefore the lift-drag ratio, are impacted by the size of the fuselage.

4 PERSPECTIVES

In the future, it is planned to add two further functionalities to the 3D aerodynamic design framework. The first feature would be to model the propulsion system using body force. The second would be to be able to perform aeroelastic calculations. This way, in the second part of the ACAP and UPWING projects, the effect of propulsion and wing deformations may be taken into account in the design of the aerodynamic shape. For the rest of the study presented in this article, it is planned to carry out multi-disciplinary optimization at the OAD level. This optimization will be based on surrogate models created from a multi-disciplinary and multi-fidelity design of experiments, presented in Figure 26. This design of experiments uses different levels of fidelity, where the goal is to explore the design space with low fidelity corrected by high fidelity calculation. The number of points in each design of experiment being inversely proportional to the computational cost of the fidelity level. For the aerodynamic part, for

example, the low-fidelity method based on an analytical model will evaluate 1280 configurations, while the CFD Euler computations will evaluate 80 configurations and the CFD RANS computations will evaluate 20 configurations.

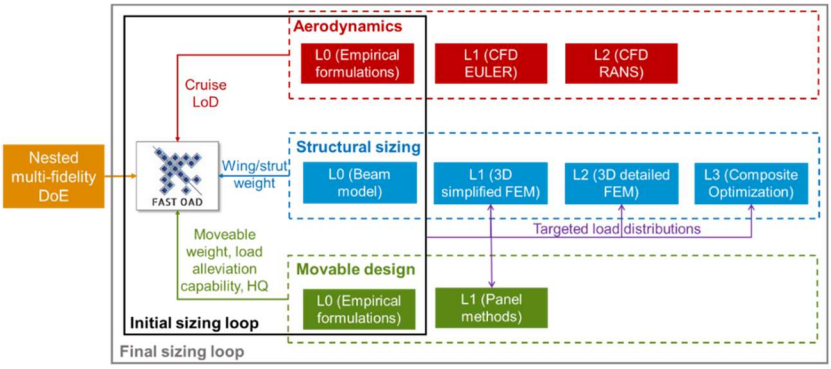

Figure 26: Multi-disciplinary and multi-fidelity design of experiments approach.

The same approach will be used for the structural design of experiments. The optimization process based on the surrogate models created from this design of experiments should provide us with the best multi-disciplinary compromise.

ACKNOWLEDGEMENT

This work and the project Ultra Performance Wing (UP Wing, project number: 101101974) is supported by the Clean Aviation Joint Undertaking and its members.

REFERENCES

[1] G. Carrier and al., "Multidisciplinary analysis and design of strut-braced wing concept for medium range aircraf," *AIAA Scitech January*, 2022.

[2] Robert, and al. Haimes, "Multi-fidelity geometry-centric multi-disciplinary analysis for design.," *AIAA Modeling and Simulation Technologies Conference*, 2016.

[3] S. Delbecq, S. Defoort, P. Schmollgruber, E. Benard, and V. Pommier-Budinger C. David, "From FAST to FAST-OAD: An open source framework for rapid Overall Aircraft Design," 2021.

[4] M. Drela, "A User's Guide to MSES, Version 3.12b," MIT Department of Aeronautics and Astronautics, Cambridge, MA, USA, 2004.

[5] Thomas D. Economon, "SU2: An Open-Source Suite for Multiphysics Simulation and Design," *AIAA Journal*, 2016.

[6] J. Van der Vooren, and D. Destarac, "Drag/thrust analysis of jet-propelled transonic transport aircraft; definition of physical drag components," *Aerospace Science and Technology, Vol. 8, No. 6*, 2004.

[7] J.E. Cooper and al., "CS2-THT U-HARWARD Project: Final Assessment and Project Outcomes Evaluation," 2024.

[8] Joaquim R. R. A. Martins Ney R. Secco, "RANS-Based Aerodynamic Shape Optimization of a Strut-Braced Wing with Overset Meshes," Journal of Aircraft, 2019.